catalysts

MDPI

Article

Cl-Modified N-Type Cu_2O Thin Films for Enhanced Photocatalytic Degradation of Norfloxacin Under Visible-Light Irradiation

Yuchen Wei [1], Qinggong Ji [2], Zongbin Liu [2], Jian Zhang [2], Lei Chen [2], Ningning Zhao [2,*] and Xiaojiao Yu [2,*]

[1] School of Materials Science and Engineering, Xi'an University of Technology, Xi'an 710048, China
[2] School of Eco-Environmental & Chemical Engineering, Xi'an University of Technology, Xi'an 710048, China
* Correspondence: zhaonn@xaut.edu.cn (N.Z.); yxjw@xaut.edu.cn (X.Y.)

Abstract

Cl-modified n-type Cu_2O thin films were prepared on indium tin oxide substrates through potentiostatic electrodeposition and investigated for the photocatalytic removal of norfloxacin (NOR). Cyclic voltammetry and X-ray diffraction identified −0.65 V and pH 5.7 as suitable deposition conditions. Cl addition regulated the nucleation and growth of Cu_2O, producing pronounced changes in crystal orientation, surface morphology, and electronic properties. The thin film obtained with 10 mmol L^{-1} KCl (Cl_{10}-Cu_2O) exhibited the strongest (111) preferred orientation and a flower-like morphology. X-ray photoelectron spectroscopy confirmed the presence of Cl species and revealed predominantly Cu^+, together with defect-associated oxygen environments and a small proportion of surface Cu^{2+}. The Mott–Schottky analysis demonstrated a transition from p-type conductivity in pristine Cu_2O to n-type behavior after Cl incorporation. The optical band gap increased from 1.94 to 2.04 eV, indicating modification of the electronic structure. Among the investigated samples, Cl_{10}-Cu_2O delivered the highest photocurrent density (0.101 mA cm^{-2}), the largest open-circuit photovoltage (11.981 mV), and the lowest interfacial charge-transfer resistance. Its apparent pseudo-first-order rate constant reached 0.00539 min^{-1}, approximately 1.61 times that of pristine Cu_2O. Scavenger experiments indicated that photogenerated holes were the predominant oxidative species, while $\cdot O_2^-$ and ·OH also participated in NOR transformation. The improved photocatalytic activity was attributed to the combined effects of conductivity-type conversion, controlled defect formation, enhanced charge separation and transfer, favorable crystal orientation, and hierarchical surface morphology.

Keywords: Cl-modified Cu_2O; n-type semiconductor; potentiostatic electrodeposition; photocatalytic degradation; norfloxacin

Check for updates

Academic Editor: Hideyuki Katsumata

Received: 10 August 2026
Revised: 12 September 2026
Accepted: 16 September 2026
Published: 18 September 2026

Copyright: © 2026 by the authors. Licensee MDPI, Basel, Switzerland. This article is an open access article distributed under the terms and conditions of the Creative Commons Attribution (CC BY) license.

1. Introduction

The widespread application of antibiotics in human healthcare, veterinary medicine, and aquaculture has resulted in their continuous release into aquatic environments, creating a significant class of emerging contaminants [1]. Unlike conventional organic pollutants, antibiotics possess strong biological activity and chemical persistence, allowing them to survive conventional wastewater treatment processes and accumulate in aquatic ecosystems. More importantly, the long-term presence of antibiotic residues can accelerate the dissemination of antibiotic-resistant bacteria and antibiotic resistance genes, posing potential risks to ecological security and public health [2–4]. Therefore, efficient removal of antibiotic contaminants from wastewater has become an urgent environmental challenge.

Among various pharmaceutical pollutants, fluoroquinolone antibiotics have attracted considerable attention due to their extensive usage and environmental persistence. Norfloxacin (NOR), a representative second-generation fluoroquinolone antibiotic, has been widely employed for treating bacterial infections in humans and animals. The stable quinolone structure, strong C-F bond, and complex functional groups endow NOR with high resistance to biodegradation, resulting in its frequent detection in hospital effluents, municipal wastewater, and natural water bodies. Even at trace concentrations, NOR may disturb microbial communities, inhibit aquatic organisms, and promote the development of antibiotic resistance [5]. Consequently, developing sustainable and highly efficient technologies for NOR degradation is of great significance for environmental remediation.

Various approaches, including adsorption, membrane separation, biological treatment, electrochemical oxidation, and advanced oxidation processes (AOPs), have been explored for antibiotic removal. In comparison, AOPs have attracted increasing interest because they can generate highly reactive species, such as hydroxyl radicals (·OH), superoxide radicals ($\cdot O_2^-$), and photogenerated holes (h^+), which are capable of oxidizing refractory organic molecules into less harmful intermediates or ultimately mineralizing them into CO_2 and H_2O [6–9]. Among various AOPs, semiconductor photocatalysis represents one of the most promising strategies because it can directly utilize solar energy, operate under mild conditions, and avoid the addition of excessive chemical oxidants [10–12]. Traditional wide-band-gap photocatalysts, such as TiO_2 and ZnO, exhibit limited visible-light utilization, which restricts their practical application under natural solar irradiation. Therefore, the development of visible-light-responsive semiconductor materials with efficient charge separation and enhanced stability has become a major research focus.

Cuprous oxide (Cu_2O), a typical p-type semiconductor with a direct band gap of approximately 2.0–2.2 eV, has emerged as a promising visible-light-driven photocatalyst. Compared with conventional metal oxides, Cu_2O possesses several advantages, including strong visible-light absorption, suitable band-edge positions, abundant elemental availability, and relatively low environmental toxicity. These characteristics enable Cu_2O to effectively utilize solar energy for photocatalytic reactions, making it attractive for applications in organic pollutant degradation, CO_2 reduction, and hydrogen evolution [13–15]. Despite these advantages, pristine Cu_2O still suffers from intrinsic limitations that hinder its practical application. The rapid recombination of photogenerated electron-hole pairs significantly decreases the number of charge carriers participating in surface reactions, resulting in insufficient photocatalytic activity. Cu_2O is vulnerable to photocorrosion because photogenerated holes can oxidize Cu^+ species into Cu^{2+} during photocatalytic reactions, causing structural degradation and loss of catalytic stability. In addition, the intrinsic p-type conductivity of Cu_2O originates mainly from copper vacancies (V_{Cu}), which can act as both active defects and recombination centers depending on their concentration. Therefore, precise regulation of the electronic structure and defect chemistry of Cu_2O is essential for achieving improved photocatalytic performance.

Elemental doping has been widely recognized as an effective strategy for tailoring semiconductor properties by modifying carrier density, defect states, band structures, and surface reaction kinetics [16–18]. Compared with complex heterojunction construction, doping engineering provides a relatively simple approach for regulating the intrinsic electronic properties of semiconductor materials [19]. In particular, donor doping offers an attractive pathway to modify the conductivity type of Cu_2O. Chlorine (Cl), as a halogen dopant with suitable atomic characteristics, has demonstrated potential for regulating the electronic structure of Cu_2O [20]. The incorporation of Cl atoms into the Cu_2O lattice can introduce donor states and increase electron concentration, thereby shifting the Fermi level and promoting the transformation from conventional p-type Cu_2O toward n-type

semiconductor behavior. Previous studies have shown that Cl doping can increase electron density, accelerate charge transport, reduce bulk recombination, and improve the utilization efficiency of photogenerated carriers [21]. The research of Nie and Zhou et al. [22,23] found that the redistribution of defect states induced by Cl incorporation may optimize surface reaction sites and enhance interfacial charge-transfer processes. The research by Chen et al. [24] indicates that Cl doping not only enhances the oxygen evolution reaction activity of Cu_2O, but also facilitates the formation of Cu vacancies. Through electronic and geometric structure regulation, the catalytic activity of $Cu_2O(111)$ can be significantly improved. Abdelfatah et al. [25] prepared n-type Cu_2O using electrochemical deposition technology. The samples exhibited higher abilities for charge carrier separation and transfer. Guan et al. [26] fabricated n-type and p-type Cu_2O using the magnetron sputtering technique for water splitting. The experimental results show that the n-type Cu_2O photoelectrode exhibits better photocurrent response. Nevertheless, most previous studies have focused on Cu_2O nanoparticles or composite photocatalysts, while systematic investigations into Cl-induced n-type conversion in Cu_2O thin films remain scarce. The relationship between Cl incorporation, defect evolution, carrier behavior, and photocatalytic degradation mechanisms requires further clarification. In addition to electronic structure regulation, catalyst configuration plays an important role in practical photocatalytic applications. Immobilized thin-film photocatalysts provide an attractive alternative because they can be easily separated from treated water. Furthermore, thin-film fabrication enables precise control over crystallinity, thickness, surface morphology, and defect distribution, which are closely associated with charge migration and catalytic activity.

Our previous studies demonstrated that doping and heterojunction construction can regulate the conductivity, band structure, and photocatalytic behavior of Cu_2O toward antibiotic contaminants [7,8,12,20]. In particular, ref. [22] established the energy-band reconstruction of Cl-doped Cu_2O and examined its application to levofloxacin degradation. Therefore, the present study does not regard either Cl-induced p-to-n conversion or the replacement of levofloxacin with another fluoroquinolone as sufficient novelty. Instead, it addresses the processing-structure-property relationship of potentiostatically electrodeposited Cl-Cu_2O thin films. The chloride concentration is systematically related to the preferred crystallographic orientation, morphology reconstruction, band configuration, and interfacial charge-transfer kinetics. Mott-Schottky, VB-XPS, optical, transient-photocurrent, open-circuit-photovoltage, and impedance measurements are jointly used to clarify why an intermediate chloride concentration produces this behavior. Norfloxacin is employed as a structurally related probe pollutant to determine whether this regulated thin-film electronic structure supports predominantly hole-mediated oxidation rather than merely reproducing the activity trend previously observed for levofloxacin. Accordingly, the contribution of this work lies in resolving the chloride-content-dependent coupling among film growth, electronic regulation, and photocatalytic function, rather than in substrate substitution alone.

Based on the above considerations, this study reports the preparation of Cl-modified n-type Cu_2O incorporation into the structural characteristics, optical properties, and electrical behavior; in addition, the photocatalytic performance of Cu_2O thin films was systematically investigated. The optimized Cl-modified Cu_2O thin films exhibited enhanced NOR degradation efficiency, owing to improved carrier separation and accelerated surface reaction kinetics. Furthermore, radical trapping experiments and degradation pathway analysis were conducted to elucidate the dominant reactive species and photocatalytic mechanism. This work provides new insights into donor-doping engineering of Cu_2O thin films

2. Results and Discussion

2.1. Investigation of Deposition Conditions for Cl-Cu_2O Thin Films and Structural Characterization

To determine an appropriate potential window for the potentiostatic electrodeposition of Cu_2O thin films, cyclic voltammetry was performed in the deposition electrolyte. As shown in Figure 1a, a pronounced cathodic reduction peak appears at approximately −0.65 V, indicating the occurrence of a substantial electrochemical reduction process. This feature can be assigned to the reduction of Cu^{2+} to Cu^{+} and the subsequent formation of Cu_2O [27]. Within the potential range from −0.30 to −0.80 V, the cathodic deposition current initially increases and then decreases as the applied potential shifts in the negative direction, demonstrating the strong dependence of Cu_2O nucleation and growth on the deposition potential. Shifting the potential negatively promotes the reduction of Cu^{2+} and increases the cathodic current, thereby facilitating Cu_2O nucleation and continuous film growth. Nevertheless, an excessively negative potential may induce the further reduction of Cu^{+} to metallic Cu. It can also result in an excessively rapid deposition rate, local depletion of electroactive species, and nonuniform nucleation [28]. Considering both the selective formation of Cu_2O and the control of film morphology, select the deposition potential as −0.65 V.

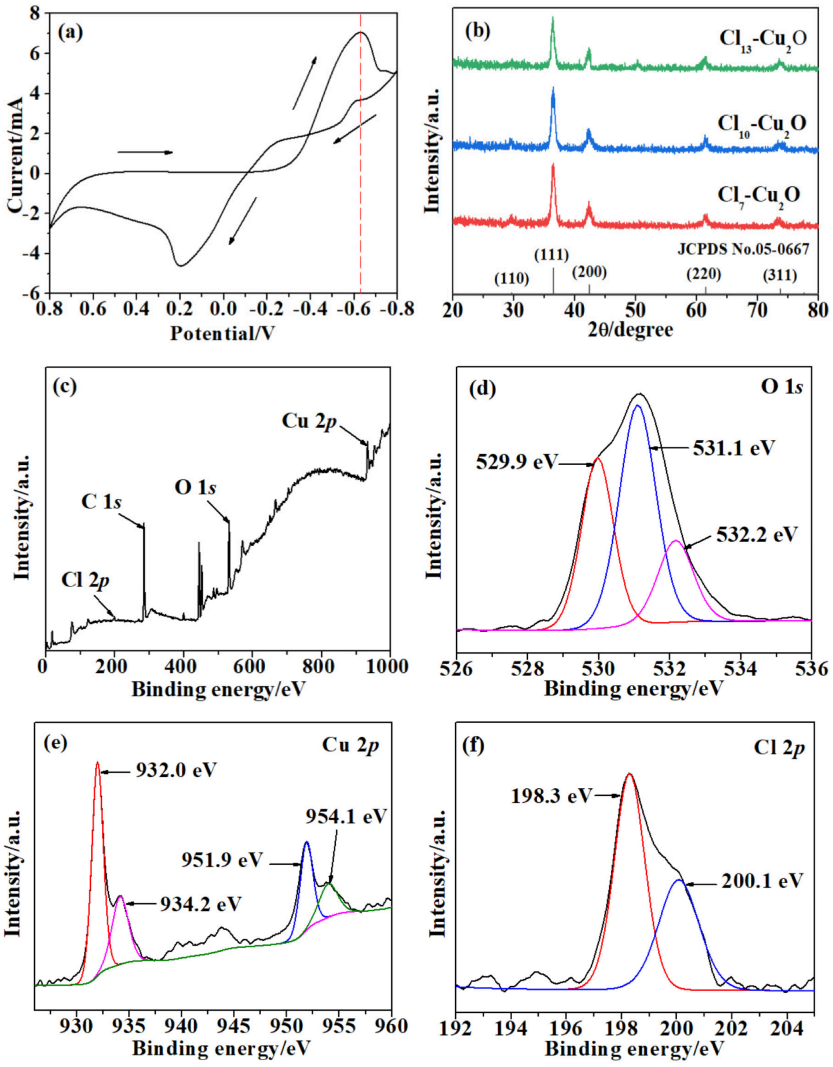


Figure 1. Cyclic voltammetry curve (**a**), XRD patterns (**b**), XPS survey spectrum (**c**), O 1s (**d**), Cu 2p (**e**), and Cl 2p (**f**) of n-Cu_2O thin film.

To clarify the influence of KCl concentration on the crystal structure of the Cu_2O thin films, XRD measurements were performed on samples electrodeposited from electrolytes containing different amounts of KCl. As shown in Figure 1b, the diffraction peaks at approximately 29.6°, 36.4°, 42.3°, 61.3°, and 73.5° can be indexed to the (110), (111), (200), (220), and (311) planes, respectively, of cubic cuprite Cu_2O. These peak positions agree well with the standard diffraction data of JCPDS No. 05-0667. No discernible reflections associated with CuO, crystalline copper chlorides, or other secondary phases are detected, indicating that the cuprite structure is retained over the investigated KCl concentration range. The (111) reflection is predominant in all three patterns, demonstrating that the electrodeposited films preferentially grow along the (111) direction. Varying the KCl concentration produces no appreciable shift in the Cu_2O reflections but noticeably changes their relative intensities. This result suggests that chloride ions primarily regulate the nucleation and orientation of Cu_2O crystallites without causing a structural change detectable by conventional XRD. When the KCl concentration is increased from 7 to 10 mmol L^{-1}, the relative intensity of the (111) reflection increases, indicating that an appropriate chloride concentration favors the development of the (111) texture. A further increase to 13 mmol L^{-1} does not provide an additional enhancement in the preferred orientation. Previous studies have demonstrated that the photocatalytic behavior of Cu_2O is strongly facet-dependent, with (111)-enriched structures frequently showing favorable surface reaction and photogenerated charge-transfer characteristics [29,30]. Accordingly, the pronounced (111) texture obtained at a KCl concentration of 10 mmol L^{-1} may contribute to improved photocatalytic performance.

X-ray photoelectron spectroscopy was employed to examine the surface elemental composition and chemical states of the optimized Cl-Cu_2O thin films. The XPS survey spectrum is presented in Figure 1c. The signals located at approximately 932 and 952 eV are assigned to Cu $2p_{3/2}$ and Cu $2p_{1/2}$, respectively, while the peak at approximately 530 eV originates from O 1s. A weak Cl 2p signal is also detected at approximately 198 eV. These results confirm that Cu, O, and Cl are present on the surface of the electrodeposited film. The detection of chlorine suggests that Cl-containing species from the electrolyte were incorporated into or retained within the Cu_2O thin film during electrodeposition, providing preliminary evidence for the involvement of Cl in film formation. The C 1s peak at approximately 284.8 eV is attributed primarily to adventitious carbon adsorbed on the sample surface and may be used as the binding-energy reference.

As shown in Figure 1d, the high-resolution O 1s spectrum was deconvoluted into three components centered at 529.9, 531.1, and 532.2 eV. The peak at 529.9 eV is assigned to lattice oxygen in the Cu-O framework of Cu_2O, whereas the component at 531.1 eV is associated with defect-related oxygen species in oxygen-deficient environments [31,32]. The higher-binding-energy peak at 532.2 eV originates mainly from surface-adsorbed oxygen-containing species, such as chemisorbed oxygen, hydroxyl groups, and molecular water. These results indicate that lattice oxygen, defect-associated oxygen, and adsorbed oxygen species coexist on the surface of the Cl-Cu_2O thin films. As shown in Figure 1e, the high-resolution Cu 2p spectrum contains two predominant peaks at 932.0 and 951.9 eV, corresponding to the Cu $2p_{3/2}$ and Cu $2p_{1/2}$ states assigned to Cu(I), respectively [33]. The spin–orbit splitting of approximately 19.9 eV is consistent with Cu_2O. Two weaker components at 934.2 and 954.1 eV are attributed to Cu(II) species [34], suggesting slight oxidation of the film surface. The low abundance and surface-localized or poorly crystalline nature of these Cu(II) species may explain the absence of detectable CuO reflections in the XRD patterns. Thus, Cu(I) constitutes the principal copper state in the film, while a minor Cu(II) contribution is present at the surface. As shown in Figure 1f, the high-resolution Cl 2p spectrum was deconvoluted into two components at 198.3 and 200.1 eV, corresponding to the Cl $2p_{3/2}$ and Cl $2p_{1/2}$ states of Cl^-, respectively [35]. Their spin–orbit separation

of approximately 1.8 eV is characteristic of ionic chloride, confirming that Cl-containing species were introduced into or retained within the Cu_2O film during electrodeposition. Although the Cl 2p signal supports the presence of chloride in the film, XPS alone cannot determine whether Cl^- substitutes for lattice oxygen or exists at grain boundaries or on the surface.

2.2. Morphological Characterization of the Cl-Cu_2O Thin Films

The influence of KCl concentration on the surface morphology and crystal-growth behavior of the Cu_2O thin films was investigated by SEM, as shown in Figure 2. In the absence of KCl, the Cu_2O thin film consists predominantly of densely packed, submicrometer pyramidal or triangular-prismatic grains (Figure 2a). The introduction of Cl substantially alters both the dimensions and architecture of the Cu_2O crystallites, indicating that Cl^- participates in regulating the nucleation process and the relative growth rates of different crystallographic facets. At a KCl concentration of 7 mmol L^{-1}, well-defined micrometer-sized flower-like crystals are formed (Figure 2b). Each hierarchical structure comprises several intergrown pyramidal or plate-like units with clearly defined edges. The crystallites are relatively uniform in size, although a small number of fine particles can be observed on their surfaces. Compared with the unmodified film, the pronounced increase in grain size suggests that an appropriate amount of Cl^- may reduce the nucleation density while promoting anisotropic crystal growth and the assembly of individual crystalline units. When the KCl concentration is increased to 10 mmol L^{-1}, the film largely retains its flower-like morphology, but the crystallites become more compactly distributed, and shallow central depressions begin to develop in some particles (Figure 2c). This observation suggests that anisotropic Cu_2O growth is maintained at this concentration, while chloride adsorption gradually modifies the relative growth rates between the central and peripheral regions of the crystallites. A further increase in KCl concentration to 13 mmol L^{-1} results in a pronounced morphological transition from flower-like crystals to concave, truncated-pyramidal or terraced structures (Figure 2d). At elevated chloride concentrations, enhanced Cu-Cl complexation and facet-selective adsorption of Cl^- may alter the availability of electroactive Cu species and the growth kinetics of individual Cu_2O facets. These effects can suppress outward growth in selected regions and favor the development of concave structures. The SEM observations therefore demonstrate that KCl concentration is a key parameter governing the grain size, surface architecture, and anisotropic growth of electrodeposited Cu_2O thin films.

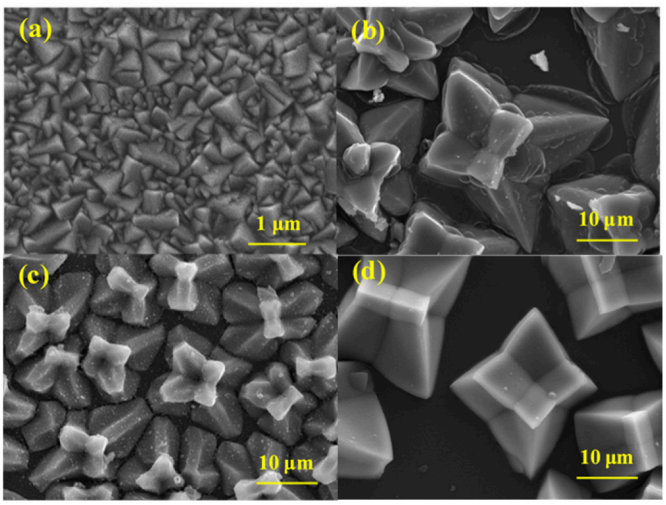


Figure 2. SEM images of Cu_2O thin films prepared with different KCl concentrations: without KCl (**a**) 7 mmol L^{-1} (**b**), 10 mmol L^{-1} (**c**), and 13 mmol L^{-1} (**d**).

2.3. Analysis of the Photoelectric Performance of Cl-Cu_2O Thin Films

Figure 3a shows the UV-Vis absorption spectra of the unmodified and Cl-containing Cu_2O thin films. All samples exhibit pronounced absorption in the visible region, consistent with the direct optical transition of Cu_2O, whose band gap is generally reported to be approximately 1.9–2.2 eV [36]. The addition of KCl noticeably changes both the absorption intensity and the position of the absorption edge. Similar variations in the optical response of electrodeposited Cu_2O have been observed following the introduction of chloride ions, which can modify the film morphology, crystallographic orientation, defect structure, and carrier concentration [37]. Considering the direct allowed optical transition of Cu_2O, the band-gap energy was estimated using the Tauc relation. Extrapolation of the linear regions in Figure 3b gives band-gap energies of approximately 1.94, 2.04, 2.03, and 2.05 eV for unmodified Cu_2O, Cl_7-Cu_2O, Cl_{10}-Cu_2O, and Cl_{13}-Cu_2O, respectively. These values are within the range commonly reported for electrodeposited Cu_2O thin films. Compared with pristine Cu_2O, all Cl-containing films show a blue shift of the absorption edge and an increase of approximately 0.09–0.11 eV in the apparent optical band gap.

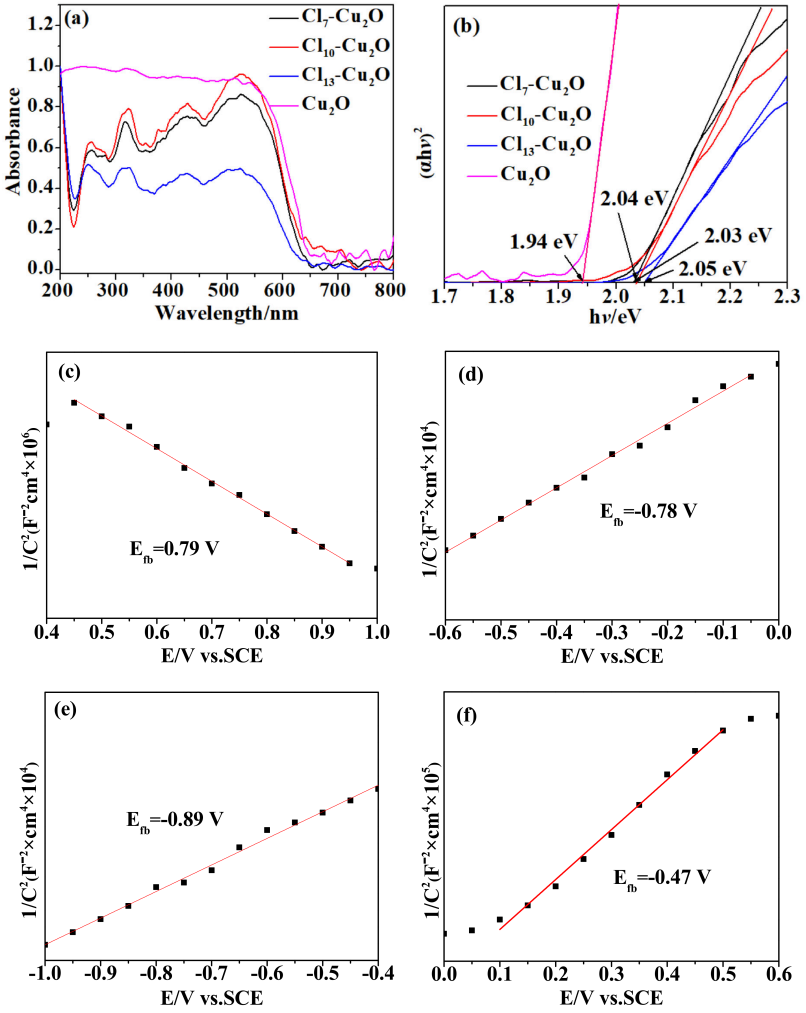


Figure 3. UV-Vis DRS (**a**), $(\alpha h\upsilon)^2$-$h\upsilon$ (**b**), and Mott–Schottky plots (Cu_2O (**c**), Cl_7-Cu_2O (**d**), Cl_{10}-Cu_2O (**e**), and Cl_{13}-Cu_2O (**f**)) of the prepared samples.

Mott–Schottky measurements were performed to determine the conductivity type and flat-band potential of the unmodified and Cl-Cu_2O thin films. As shown in Figure 3c, the unmodified Cu_2O thin films exhibit a negative Mott–Schottky slope, confirming p-type conductivity with holes as the majority carriers. Linear fitting gives a flat-band potential (E_{FB})

of 0.79 V vs. SCE. The p-type behavior of unmodified Cu_2O is generally associated with intrinsic acceptor defects, particularly copper vacancies. In contrast, the Mott–Schottky plots of Cl_7-Cu_2O, Cl_{10}-Cu_2O, and Cl_{13}-Cu_2O all display positive slopes (Figure 3d–f), demonstrating a conversion from p-type to n-type conductivity following the addition of KCl. Together with the Cl 2p XPS results, the positive slopes provide evidence that chloride incorporation alters the electronic properties of the Cu_2O films. The E_{FB} of Cl_7-Cu_2O, Cl_{10}-Cu_2O, and Cl_{13}-Cu_2O were determined to be −0.78, −0.89, and −0.47 V vs. SCE, respectively. The Mott–Schottky plots recorded at 1000 Hz show a negative slope for pristine Cu_2O and positive slopes for the Cl-doped Cu_2O films. Within the limitations of this single-frequency measurement, this change in slope direction suggests that Cl incorporation induces a transition from predominantly p-type to n-type-like semiconductor behavior. The conventional carrier-density calculation was not applied because the electrodeposited films have rough, morphology-dependent interfaces and may exhibit contributions from surface states, defect-related capacitance and frequency dispersion. Therefore, the measured capacitance does not necessarily represent an ideal depletion-layer capacitance, and carrier densities derived using the geometric electrode area may be physically unrealistic. Accordingly, the Mott–Schottky plots are used here only for qualitative determination of semiconductor conductivity type and estimation of flat-band potentials, rather than for quantitative determination of bulk carrier concentrations.

The transient photocurrent responses of the Cu_2O thin films prepared with different KCl concentrations were measured under periodically interrupted illumination. As shown in Figure 4a, all samples exhibit reproducible current changes synchronized with the light on/off cycles. The current increases rapidly upon illumination and returns toward its initial level after the light is switched off, confirming the photoresponsive nature of the electrodeposited films. The photocurrent-density increments of unmodified Cu_2O, Cl_7-Cu_2O, Cl_{10}-Cu_2O, and Cl_{13}-Cu_2O are approximately 0.012, 0.020, 0.101, and 0.028 mA cm^{-2}, respectively. Cl_{10}-Cu_2O exhibited the largest photocurrent response, approximately 8.4, 5.1, and 3.6 times those of Cu_2O, Cl_7-Cu_2O, and Cl_{13}-Cu_2O, respectively. The preservation of the response over successive illumination cycles also indicates satisfactory short-term photoelectrochemical reproducibility. The enhanced photocurrent of Cl_{10}-Cu_2O indicates that a larger proportion of the photogenerated carriers can be separated and collected at the external circuit. This improvement may arise from the Cl^- induced conductivity-type conversion, increased donor density, and favorable changes in crystallographic orientation and surface morphology. In contrast, increasing the KCl concentration to 13 mmol L^{-1} decreases the photocurrent response. Excessive chloride incorporation may introduce additional defect or trapping states and modify the morphology and optical absorption of the film, thereby limiting effective carrier transport. Combined with the optical and Mott–Schottky results, these findings identify 10 mmol L^{-1} as the appropriate KCl concentration for promoting photogenerated charge separation and transport in the n-type Cu_2O thin films.

The open-circuit potential responses of the Cl-Cu_2O thin films were measured under periodically interrupted illumination to evaluate the influence of KCl concentration on photogenerated-carrier accumulation and recombination. As shown in Figure 4b, all samples exhibit regular potential variations synchronized with the light on/off cycles. The reproducible responses over successive cycles demonstrate the stable photoelectrochemical behavior of the electrodeposited films. The open-circuit photovoltage variation of unmodified Cu_2O is 3.243 mV. After the introduction of KCl, the corresponding values increase to 4.212, 11.981, and 8.677 mV for Cl_7-Cu_2O, Cl_{10}-Cu_2O, and Cl_{13}-Cu_2O, respectively. Thus, Cl_{10}-Cu_2O produces the largest photovoltage, approximately 3.69 times that of unmodified Cu_2O and 2.84 and 1.38 times those of Cl_7-Cu_2O and Cl_{13}-Cu_2O, respectively.

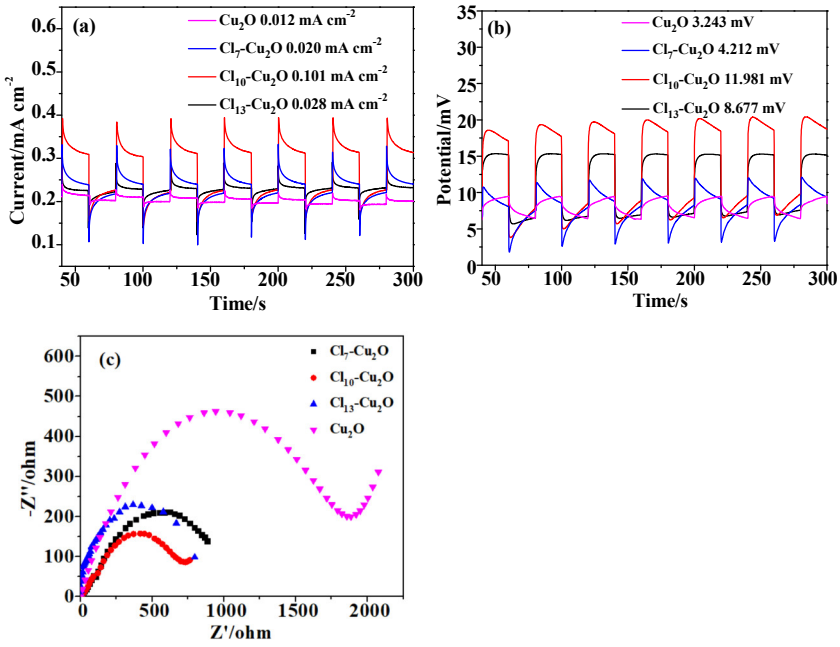


Figure 4. Transient photocurrent responses (**a**), open-circuit potential responses (**b**), Nyquist plots (**c**) of the prepared Cl-Cu_2O thin films.

The open-circuit photovoltage originates from the light-induced separation of the electron and hole quasi-Fermi levels. The larger photovoltage of Cl_{10}-Cu_2O indicates that a more pronounced photoinduced potential can be established in this film, suggesting favorable carrier accumulation and interfacial charge-separation behavior. This result agrees with the enhanced transient photocurrent obtained from the Mott–Schottky analysis, supporting the beneficial effect of adding 10 mmol L^{-1} KCl on the photoelectrochemical properties of Cu_2O.

Figure 4c presents the Nyquist plots of unmodified Cu_2O and the Cl-Cu_2O thin films. The unmodified Cu_2O electrode exhibits the largest impedance arc, whereas all Cl-containing samples show smaller arc diameters. A smaller Nyquist arc is generally associated with a lower interfacial charge-transfer resistance (R_{ct}). Dopant incorporation decreased R_{ct} and improved the photoelectrochemical charge-transfer characteristics relative to unmodified Cu_2O [38]. Among the Cl-containing electrodes, Cl_{10}-Cu_2O exhibits the smallest impedance arc, indicating the most favorable charge-transfer kinetics at the electrode/electrolyte interface. This behavior may originate from the combined effects of Cl-induced n-type conductivity and the pronounced (111) preferred orientation [39]. The strong (111) texture of Cl_{10}-Cu_2O may therefore contribute to its relatively low interfacial resistance. Together with the enhanced photocurrent and open-circuit photovoltage, the EIS results indicate that Cl_{10}-Cu_2O provides the most favorable carrier collection and interfacial-transfer behavior among the investigated films.

2.4. Analysis of the Photocatalytic Performance of Cl-Cu_2O Thin Films

The photocatalytic activity of the Cl-Cu_2O thin films was evaluated using NOR as the target contaminant, as shown in Figure 5. After 30 min of dark adsorption, the characteristic absorption peak of NOR at approximately 270 nm gradually decreased with increasing irradiation time (Figure 5a). The absorption band at approximately 320–330 nm also weakened progressively, indicating continuous depletion of NOR and disruption of its conjugated structure and chromophoric groups during photocatalysis. As shown in Figure 5b, only approximately 13% of NOR was removed after 180 min in the absence of a photocatalyst, demonstrating that direct photolysis made a relatively minor contribution. The NOR removal

efficiency over the pristine Cu_2O film was 52.3%, whereas those obtained with the Cl_7-Cu_2O, Cl_{10}-Cu_2O, and Cl_{13}-Cu_2O thin films reached 62.2%, 67.3%, and 64.5%, respectively. These results demonstrate that appropriate Cl doping improves the photocatalytic activity of Cu_2O. Among the investigated films, Cl_{10}-Cu_2O exhibited the highest NOR removal efficiency, compared with pristine Cu_2O, representing an increase of 15.0 percentage points. The superior performance of Cl_{10}-Cu_2O is consistent with its enhanced photoresponse, higher photocurrent, and lower interfacial charge-transfer resistance, suggesting more effective charge transport and utilization at the film-solution interface. Its pronounced (111) preferred orientation and favorable surface morphology may also increase the availability of surface sites for NOR oxidation. When the KCl concentration was further increased to 13 mmol L^{-1}, the photocatalytic efficiency decreased slightly. This decline may be associated with excessive defect formation, morphology reconstruction, or the introduction of additional charge-recombination sites. Accordingly, the effect of Cl doping is not linearly proportional to the KCl concentration, and 10 mmol L^{-1} represents the KCl addition level within the investigated range. The degradation kinetics of NOR over the different films were further evaluated using the pseudo-first-order kinetic model. As shown in Figure 5c, $\ln(c_0/c_t)$ increases approximately linearly with irradiation time. The apparent rate constants obtained for Cu_2O, Cl_7-Cu_2O, Cl_{10}-Cu_2O, and Cl_{13}-Cu_2O were 0.00335, 0.00516, 0.00539, and 0.00503 min^{-1}, respectively. All the Cl-Cu_2O thin films exhibited higher rate constants than pristine Cu_2O, confirming that appropriate Cl incorporation accelerates NOR degradation. Cl_{10}-Cu_2O displayed the highest k_{app}, reaching 0.00539 min^{-1} with $R^2 = 0.9906$, which was approximately 1.61 times that of pristine Cu_2O. This kinetic result is consistent with its superior NOR removal efficiency and suggests that an appropriate Cl content favors photogenerated charge transport and interfacial reaction kinetics. When the KCl concentration was increased beyond 13 mmol L^{-1}, k_{app} decreased to 0.00503 min^{-1} for Cl_{13}-Cu_2O. The decline indicates that excessive Cl addition does not continuously enhance the reaction rate, possibly because excessive defect formation, surface-site alteration, or morphology reconstruction promotes charge recombination. These findings demonstrate that an appropriate chloride concentration can regulate the electronic and interfacial properties of electrodeposited Cu_2O thin films and improve their initial NOR removal performance. Long-term photocorrosion resistance, compositional retention, and reusability remain to be established through cycling, post-reaction characterization, and leaching analyses. The present study evaluates the initial photocatalytic and photoelectrochemical performance of the Cl-Cu_2O thin films but does not establish their long-term stability.

Reactive-species-trapping experiments were conducted to identify the principal species involved in the photocatalytic degradation of NOR over the Cl-Cu_2O thin films. Methanol (MT), benzoquinone (BQ), and isopropanol (IPA) were employed as scavengers for h^+, $\cdot O_2^-$, and $\cdot OH$, respectively. As shown in Figure 5d, the characteristic NOR absorption peak at approximately 270 nm gradually decreased in the presence of MT; however, its attenuation was markedly suppressed. The NOR degradation efficiency reached only 46.6% after 180 min, confirming that the corresponding oxidation pathway made an important contribution to the reaction. As illustrated in Figure 5e, approximately 62% of NOR was degraded after 180 min without a scavenger. Following the addition of MT, BQ, and IPA, the degradation efficiencies decreased to approximately 46.6%, 50.0%, and 56.0%, respectively. The inhibition observed for all three scavengers indicates that h^+, $\cdot O_2^-$, and $\cdot OH$ are involved in NOR degradation. MT produced the strongest suppression, suggesting that the h^+-mediated oxidation pathway plays a predominant role. The substantial inhibition caused by BQ identifies $\cdot O_2^-$ as another important reactive species, whereas the comparatively weaker effect of IPA indicates a more limited contribution from $\cdot OH$. Accordingly, the relative importance of the reactive species can be tentatively ranked as $h^+ > \cdot O_2^- > \cdot OH$ under the present conditions.

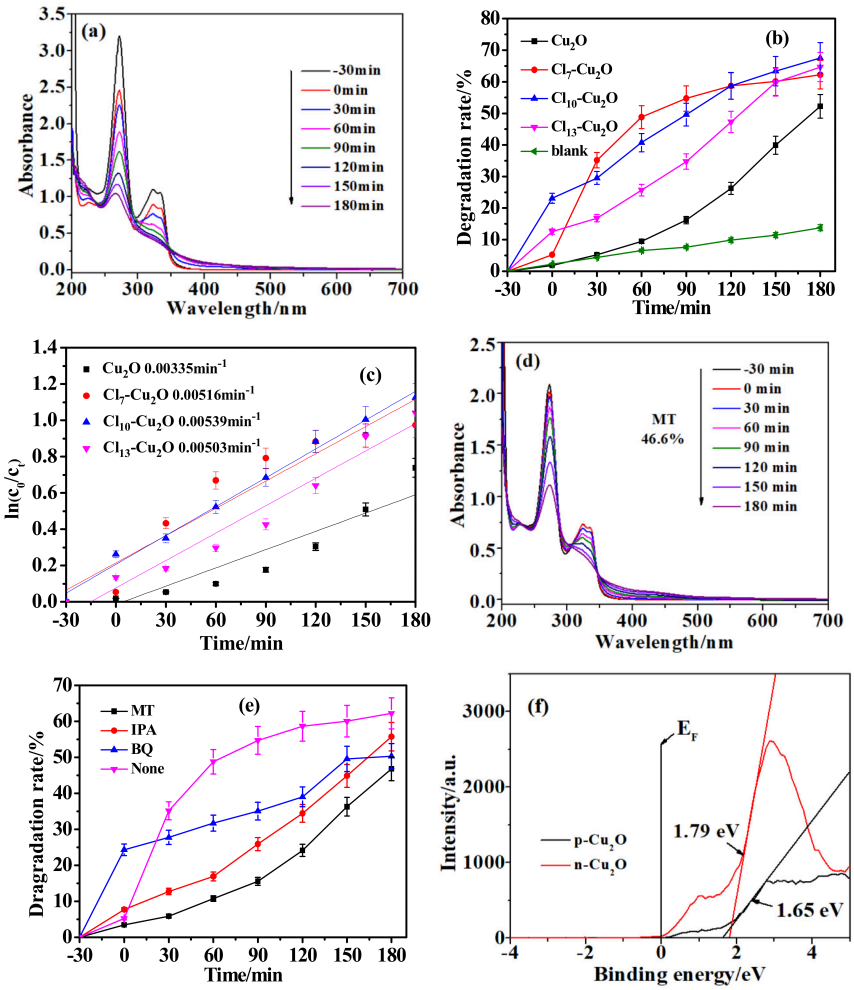


Figure 5. UV-visible absorption graph (**a**), degradation rate curve (**b**), kinetic curve (**c**), quenching experiment (**d**,**e**) of Cl-Cu_2O thin films for NOR, VB XPS pattern (**f**) of Cu_2O and Cl_{10}-Cu_2O thin films.

VB-XPS was employed to investigate the occupied valence-band electronic states and determine the energy separation between the valence-band maximum and the Fermi level [40]. As shown in Figure 5f, linear extrapolation of the valence-band edges yielded EF-EVBM values of 1.65 and 1.79 eV for pristine and Cl-doped Cu_2O, respectively. The increased separation after Cl incorporation indicates a modification of the near-valence-band electronic structure and the relative position of the Fermi level. The observable shift of the valence band edge toward higher binding energy. It indicates a downward movement of the valence band, which increases the optical band gap [40,41].

The conduction-band positions were estimated from the flat-band potentials obtained from the Mott–Schottky plots. The measured flat-band potentials versus SCE were converted to the NHE scale using Equation (1):

$$E_{FB}(NHE) = E_{FB}(SCE) + 0.241\ V \quad (1)$$

For the n-type Cl-doped Cu_2O films, the conduction-band potentials were estimated by assuming that the conduction-band minimum lies approximately 0.10 V more negative than the flat-band potential:

$$E_{CB}(NHE) \approx E_{FB}(NHE) - 0.10\ V \quad (2)$$

For p-type Cu_2O, the flat-band potential is located close to the valence-band edge. Accordingly, the valence-band potential was first estimated using:

$$E_{VB}(NHE) \approx E_{FB}(NHE) + 0.10\ V \quad (3)$$

Based on these relationships, the estimated valence-band potentials of Cu_2O, Cl_7-Cu_2O, Cl_{10}-Cu_2O, and Cl_{13}-Cu_2O were +1.13, +1.40, +1.28, and +1.72 V vs. NHE, respectively, while their corresponding conduction-band potentials were −0.81, −0.64, −0.75, and −0.33 V vs. NHE, respectively. These values should be regarded as estimated band-edge potentials because they depend on the assumed 0.10 V offset between the flat-band potential and the nearest band edge. The estimated band-edge potentials indicate that Cl incorporation modifies both the oxidative ability of valence-band holes and the reductive ability of conduction-band electrons. Pristine Cu_2O possesses the most negative conduction-band potential (−0.81 V vs. NHE), but its relatively low valence-band potential (+1.13 V) and inefficient charge separation limit its overall photocatalytic activity. Among the Cl-doped films, Cl_{10}-Cu_2O exhibits the most negative conduction-band potential (−0.75 V), providing a favorable thermodynamic driving force for interfacial oxygen reduction and the formation of $\cdot O_2^-$. Its valence-band potential (+1.28 V) can also support the direct oxidation of NOR by photogenerated holes. Together with its enhanced photocurrent response, higher photovoltage and lower interfacial charge-transfer resistance, this balanced band configuration accounts for the superior photocatalytic activity of Cl_{10}-Cu_2O. Although Cl_{13}-Cu_2O has the most positive valence-band potential (+1.72 V), its conduction band shifts positively to −0.33 V, substantially decreasing the driving force for oxygen reduction. Therefore, the photocatalytic performance is governed by the combined effects of band-edge positions and charge-carrier kinetics rather than by the oxidation or reduction potential alone.

2.5. Analysis of the Mechanism of Cl-Cu_2O Thin Films Enhancing Photocatalytic Degradation of NOR

The enhanced photocatalytic activity of the Cl-Cu_2O thin films can be attributed to the synergistic effects of conductivity-type conversion, defect regulation, improved charge separation, and accelerated interfacial charge transfer. Cl incorporation introduces donor-like electronic states and shifts the Fermi level toward the conduction band, resulting in the conversion of Cu_2O from p-type to n-type conductivity and an increase in the apparent electron-carrier density. Although the enlarged optical band gap does not itself demonstrate suppressed charge recombination, the enhanced photocurrent and photovoltage responses, together with the reduced interfacial charge-transfer resistance, provide evidence for more efficient charge separation, collection, and interfacial utilization. Appropriate defect sites may temporarily trap photogenerated electrons and delay their recombination with holes. In addition, the pronounced (111) orientation and flower-like morphology of Cl_{10}-Cu_2O increase the accessibility of surface reaction sites and facilitate interfacial mass and charge transfer. These combined structural and electronic effects account for the superior NOR degradation efficiency of the optimized Cl_{10}-Cu_2O thin films.

Based on the results of the active species capture experiments and the relevant literature [42–45], a possible catalytic mechanism is proposed, as shown in Equations (4)–(8). Under light irradiation, Cl-Cu_2O absorbs incident photons and generates electron-hole pairs. The photogenerated holes can directly oxidize NOR molecules adsorbed on the film surface. They may also react with surface-bound H_2O or OH^- to produce highly oxidative hydroxyl radicals. Meanwhile, photogenerated electrons can participate in the activation of dissolved oxygen, producing superoxide radicals or other reactive oxygen

species. Reactive species-trapping experiments indicate that h^+, $\cdot O_2^-$, and ·OH are involved in NOR degradation.

$$Cl\text{-}Cu_2O + h\nu \rightarrow e^- + h^+ \quad (4)$$

$$h^+ + H_2O \rightarrow \cdot OH + H^+ \quad (5)$$

$$h^+ + OH^- \rightarrow \cdot OH \quad (6)$$

$$e^- + O_2 \rightarrow \cdot O_2^- \quad (7)$$

$$h^+ + \cdot OH + \cdot O_2^- + NOR \rightarrow \text{degradation products} \quad (8)$$

These findings suggest that direct oxidation mediated by photogenerated holes constitutes the predominant pathway for NOR degradation, while $\cdot O_2^-$ and ·OH contribute to the subsequent transformation of NOR and its intermediates. This interpretation is consistent with reaction mechanisms previously reported for the photocatalytic treatment of fluoroquinolone antibiotics [7,22]. Under sufficiently prolonged reaction conditions, these intermediates may undergo further oxidation and eventual mineralization.

3. Experimental

3.1. Chemicals and Reagents

Copper (II) acetate ($Cu(CH_3COO)_2$), sodium acetate (CH_3COONa), potassium chloride (KCl), absolute ethanol (CH_3CH_2OH), acetone (CH_3COCH_3), and norfloxacin (NOR, $C_{16}H_{18}FN_3O_3$) were purchased from Sinopharm Chemical Reagent Co., Ltd. All chemicals were of analytical grade and used without further purification. Deionized water was used throughout all experimental procedures.

3.2. Preparation of Cl-Modified Cu_2O Thin Films

(1) Pretreatment of ITO substrates

Indium tin oxide (ITO) conductive glass substrates (sheet resistance $\leq 15\ \Omega/\square$) were used as the deposition substrates. The ITO glasses were cut into pieces with dimensions of 1 × 2 cm and sequentially ultrasonically cleaned in acetone, ethanol, and deionized water for 20 min each. After cleaning, the substrates were dried in an oven and stored for subsequent electrodeposition.

(2) Fabrication of Cl-modified Cu_2O thin films

The Cl-modified Cu_2O thin films were prepared by a potentiostatic electrodeposition method using a conventional three-electrode electrochemical system. A mixed solution containing 0.02 mol L^{-1} $Cu(CH_3COO)_2$ and 0.1 mol L^{-1} CH_3COONa with a volume ratio of 1:1 was employed as the electrolyte. Different amounts of KCl solution were subsequently introduced into the electrolyte as the chlorine source. The pH value of the deposition solution was adjusted to 5.7. The electrodeposition process was performed at a constant potential of −0.65 V for 60 min. After deposition, the obtained thin films were carefully removed from the electrolyte, rinsed three times with deionized water, and dried at 60 °C. The resulting Cl-modified Cu_2O thin films were denoted as Cl-Cu_2O. By adjusting the KCl concentration to 7, 10, and 13 mmol L^{-1}, the corresponding samples were labeled as Cl_7-Cu_2O, Cl_{10}-Cu_2O, and Cl_{13}-Cu_2O, respectively.

3.3. Characterization of Microstructure and Photoelectrochemical Properties

The crystal structure of the Cl-modified Cu_2O thin films was characterized using an X-ray diffractometer (XRD-6100, Shimadzu, Kyoto, Japan). Their surface chemical composition and bonding states were examined by X-ray photoelectron spectroscopy (K-

Alpha, Thermo Fisher Scientific, Waltham, MA, USA), while the surface morphology was observed using a scanning electron microscope (SEM, TESCAN, Brno, Czech Republic). The optical properties were investigated by UV-Vis diffuse reflectance spectroscopy (UV-3600, Shimadzu, Japan).

The photoelectrochemical properties of the thin films were evaluated using an electrochemical workstation in a conventional three-electrode configuration in a 0.5 mol L^{-1} Na_2SO_4 aqueous solution. The Cl-Cu_2O thin film served as the working electrode, with an electrochemically exposed area of 3.0 cm^2(1.5 cm × 2.0 cm). A Pt plate and a saturated calomel electrode (SCE) were used as the counter and reference electrodes, respectively. The measurements were performed in a self-made sealed box, with a 250 W xenon lamp as the light source. The small holes of the box were covered with shading cardboard, and the light was turned on and off at 20 s intervals to measure the relationship between the current of the Cl-Cu_2O film and time, as well as the relationship between the potential and time. The AC impedance and Mott–Schottky curve of the sample were measured under these dark conditions at 1000 Hz. However, because the capacitance response of electrodeposited thin films may be affected by surface states, interfacial capacitance, film roughness, and measurement frequency, the slopes are not used to calculate or compare bulk carrier concentrations. Transient photocurrent, open-circuit potential, Mott–Schottky, and electrochemical impedance spectroscopy measurements were performed to assess the photogenerated-carrier response, semiconductor conductivity type, flat-band potential, and interfacial charge-transfer behavior.

3.4. Evaluation of Photocatalytic Performance

The photocatalytic activity of the prepared Cu_2O thin films was evaluated using NOR as the target contaminant. Each thin film was placed in a quartz tube containing 50 mL of a 10 mg L^{-1} NOR solution. A 300 W xenon lamp equipped with a 420 nm cut-off filter was used as the visible-light source, and the reaction temperature was maintained at 25 °C. Before illumination, the reaction system was kept in the dark for 30 min to establish adsorption–desorption equilibrium. The suspension was subsequently irradiated for 3 h, and aliquots were collected at 30 min intervals. The absorbance of each collected solution was measured using a UV-Vis spectrophotometer, and the NOR concentration was determined from a previously established calibration curve. The apparent NOR removal efficiency was calculated from the decrease in absorbance at 270 nm. This spectrophotometric method monitors the attenuation of the characteristic NOR absorption band but does not quantify mineralization or identify transformation products. All quantitative photocatalytic results were obtained using three independently prepared Cl-Cu_2O thin films under identical conditions.

3.5. Activity Species Trapping Test

Reactive species trapping experiments were conducted under the same conditions as the photocatalytic activity tests. Methanol (MT), p-benzoquinone (BQ), and isopropanol (IPA) were used as scavengers for hole (h^+), superoxide radicals ($\cdot O_2^-$), and hydroxyl radicals (·OH), respectively. Before dark equilibration, the scavenger solution was added to 50 mL of a 10 mg L^{-1} NOR solution to obtain a final scavenger concentration of 10 mmol L^{-1}. The total reaction volume was maintained at 50 mL in all experiments. A scavenger-free system was tested in parallel as the control.

4. Conclusions

Cl-modified n-type Cu_2O thin films were successfully fabricated by potentiostatic electrodeposition. The optimized Cl_{10}-Cu_2O film exhibited pronounced (111) preferred

orientation, a flower-like morphology, and a Cl-regulated surface defect structure. Mott–Schottky analysis confirmed that Cl incorporation converted Cu_2O from p-type to n-type conductivity. This electronic regulation improved photogenerated-carrier separation and interfacial transfer, as evidenced by the enhanced photocurrent and photovoltage responses and the reduced charge-transfer resistance.

Cl_{10}-Cu_2O achieved an NOR degradation efficiency of 67.3% and an apparent rate constant of 0.00539 min^{-1}, outperforming pristine Cu_2O. Scavenger experiments indicated that h^+ was the predominant active species, while $\cdot O_2^-$ and ·OH also contributed to NOR transformation. The improved activity originated from the synergistic effects of conductivity-type conversion, controlled defect formation, favorable crystal orientation, and accelerated charge transfer. These findings demonstrate that appropriate chloride modification provides an effective route for improving Cu_2O thin-film photocatalysts for antibiotic-contaminated water treatment.

Author Contributions: Y.W.: writing—review and editing, data curation. Q.J.: writing—original draft, data curation. Z.L.: formal analysis, data curation. J.Z.: formal analysis. L.C.: formal analysis. N.Z.: writing—review and editing, supervision. X.Y.: resources, project administration. All authors have read and agreed to the published version of the manuscript.

Funding: This research received no external funding.

Data Availability Statement: The original contributions presented in this study are included in the article. Further inquiries can be directed to the corresponding authors.

Acknowledgments: This work was financially supported by the National Natural Science Foundation of China (No. 22578360), the State Key Laboratory of Water Engineering Ecology and Environment in Arid Area (No. SKL-ZZ03-2025-06), and the Natural Science Basic Research Program of Shaanxi Province (No. 2025JC-YBMS-157).

Conflicts of Interest: The authors declare no conflicts of interests.

References

1. Kümmerer, K. Antibiotics in the aquatic environment-A review-Part I. *Chemosphere* **2009**, *75*, 417–434. [PubMed]
2. Martinez, J.L. Environmental pollution by antibiotics and by antibiotic resistance determinants. *Environ. Pollut.* **2009**, *157*, 2893–2902. [CrossRef] [PubMed]
3. Michael, I.; Rizzo, L.; McArdell, C.S.; Manaia, C.M.; Merlin, C.; Schwartz, T.; Dagot, C.; Fatta-Kassinos, D. Urban wastewater treatment plants as hotspots for the release of antibiotics in the environment: A review. *Water Res.* **2013**, *47*, 957–995. [CrossRef] [PubMed]
4. der Beek, T.A.; Weber, F.A.; Bergmann, A.; Hickmann, S.; Ebert, I.; Hein, A.; Küster, A. Pharmaecuticals in the environment-global occurrences and perspectives. *Environ. Toxicol. Chem.* **2016**, *35*, 823–835. [CrossRef] [PubMed]
5. Grenni, P.; Ancona, V.; Caracciolo, A.B. Ecological effects of antibiotics on natural ecosystems: A review. *Microchem. J.* **2018**, *136*, 25–39. [CrossRef]
6. Zhang, Q.; Zheng, D.; Bai, B.; Ma, Z.; Zong, S. Insight into antibiotic removal by advanced oxidation processes (AOPs): Performance, mechanism, degradation pathways, and ecotoxicity assessment. *Chem. Eng. J.* **2024**, *500*, 157134. [CrossRef]
7. Liu, Z.; Yu, X.; Wang, K.; Zhang, J.; Niu, J. Introducing oxygen cacancies to tune Cu_2O by Sn ion-modified for high-effective photocatalytic degradation of norfloxacin in wastewater. *Sep. Purif. Technol.* **2025**, *356*, 129810. [CrossRef]
8. Wei, Y.; Ji, Q.; Wang, K.; Zhang, J.; Niu, J.; Yu, X. Preparation and photoelectric properties of Pr-modified p-Cu_2O thin films photocatalyst based on energy band structure regulation. *Molecules* **2023**, *28*, 7560. [CrossRef] [PubMed]
9. Humayun, M.; Li, Z.S.; Israr, M.; Khan, A.; Luo, W.; Wang, C.D.; Shao, Z.P. Perovskite type ABO_3 oxides in photocatalysis, electrocatalysis, and solid oxide fuel cells: State of the art and future prospects. *Chem. Rev.* **2025**, *125*, 3165–3241. [CrossRef] [PubMed]
10. Sayed, M.; Qi, K.; Wu, X.; Zhang, L.; Garcia, H.; Yu, J. Cu-based S-scheme photocatalysts. *Chem. Soc. Rev.* **2025**, *54*, 4874–4921. [CrossRef] [PubMed]

11. Liu, Z.; Yu, X.; Wei, Y.; Wang, K.; Zhang, M.; Liu, J.; Chen, L.; Zhang, J.; Niu, J. Investigation of the photoelectric properties of nanostructured CeO_2/Cu_2O heterojunction: Photocatalytic degradation of sulfadiazine in water. *Environ. Res.* **2025**, *268*, 120788. [CrossRef] [PubMed]
12. Yu, X.; Liu, Z.; Chen, Y.; Zhao, N.; Chen, L.; Liu, N. Co-doping regulation of the band structure and carrier behavior of Cu_2O thin films and their photocatalytic degradation performance toward antibiotics. *J. Electrochem. Soc.* **2026**, *173*, 072505. [CrossRef]
13. Wang, R.; Yu, X.; Liu, Z.; Zhang, J.; Wei, Y.; Niu, J. From Mo^{4+}-induced heterojunction construction to Mo^{6+}-boosted charge transfer: A stepwise strategy for high-performance MoO_2/Cu_2O visible-light catalysts. *Chem. Mater.* **2026**, *38*, 4191–4206.
14. Paracchino, A.; Laporte, V.; Sivula, K.; Grätzel, M.; Thimsen, E. Highly active oxide photocathode for photoelectrochemical water reduction. *Nat. Mater.* **2011**, *10*, 456–461. [CrossRef] [PubMed]
15. Ma, D.; Kong, X.; You, X.; Liu, L.; Bao, R.; Cui, H.; Liu, F.; Yi, J. Bi single-atom decorated Cu/Cu_2O heterostructure via spray pyrolysis for 100% selectivity in photocatalytic CO production. *Chem. Eng. J.* **2026**, *530*, 173814. [CrossRef]
16. Minh, D.T.N.; Thien, T.D.; Cham, L.T.M.; Thanh, H.V.; Quan, N.D.T.; Cuong, N.D.; Anh, H.T.; Lam, N.D. Site-selective Yb and/or Co doping in Cu_2O/ZnO heterostructures for enhanced photocatalytic removal of dye and antibiotic pollutants. *Ceram. Int.* **2026**, *52*, 29060–29073. [CrossRef]
17. Kang, K.; Wang, Q.; Huang, H.; Zhuang, X.; Cai, J.; Wang, T.; Wang, X.; Xie, Z.; Xie, S. Tailoring surface charge distribution via lattice Cl-doping on Cu_2O nanocubes for high-selectivity CO_2-to-C_{2+} electroreduction via asymmetric C-C coupling. *Sci. China-Chem.* **2026**, *69*, 217–224. [CrossRef]
18. Liu, X.; Pei, Y.; Mao, X.; Xu, Y.; Li, Y.; Yang, H. The critical role of S-doping in the selective removal of oxytetracycline by activated peroxymonosulfate. *J. Environ. Chem. Eng.* **2025**, *13*, 117693. [CrossRef]
19. Abadi, A.G.; AlSaidi, M.S.; Shibli, W.K.A. DFT-driven approaches to optimizing small bandgap doping structures: A brief review. *J. Inorg. Organomet. Polym. Mater.* **2025**, *35*, 6130–6146. [CrossRef]
20. Yu, X.; Tian, Y.; Wei, Y.; Wang, K.; Liu, Z.; Yang, F.; Chen, L.; Zhang, J. Constructing p-n heterojunctions of Cl-Cu_2O and PANI on three-dimensional nanofiber networks for enhanced photocatalytic degradation of oxytetracycline. *J. Alloys Compd.* **2024**, *1005*, 175998. [CrossRef]
21. Khellaf, N.; Herbadji, A.; Rabhi, S.; Bouderbala, I.Y.; Aitbara, A.; Cherifi, A.; Kheloufi, S.; Bouras, I.E. Understanding and unveiling the role of chlorine potassium concentration in electrochemical nucleation, growth, and properties of p-type Cu_2O thin films. *J. Electrochem. Soc.* **2025**, *172*, 052501. [CrossRef]
22. Nie, J.; Yu, X.; Liu, Z.; Zhang, J.; Ma, Y.; Chen, Y.; Ji, Q.; Zhao, N.; Chang, Z. Energy band reconstruction mechanism of Cl-modified Cu_2O and photocatalytic degradation pathway for levofloxacin. *J. Clean. Prod.* **2022**, *363*, 132593. [CrossRef]
23. Zhou, L.; Wen, Z.; Cui, L.; Yang, G.; Luo, Y.; Xie, Y.; Cui, C.; Li, C.; Fu, G. Investigating the mechanism of propylene epoxidation over halogen (X = F, Cl, Br, I) modified Cu_2O (110) surfaces: A theoretical study. *Catal. Sci. Technol.* **2024**, *14*, 928–934. [CrossRef]
24. Chen, H.H.; Ji, Y.; Fan, T. Understanding the role of Cl doping in the oxygen evolution reaction on cuprous oxide by DFT. *Phys. Chem. Chem. Phys.* **2022**, *24*, 25347–25355. [CrossRef] [PubMed]
25. Abdelfatah, M.; Darwesh, N.; Atta, H.; Beltagi, A.M.; Sun, B.; El-Shaer, A.; Ismail, W. Inverting electrodeposited nanostructured Cu_2O thin films from n-type to p-type semiconductors and variation of their physical and photoelectrochemical properties for optoelectronic applications. *Ceram. Int.* **2023**, *49*, 30732–30743. [CrossRef]
26. Guan, L.; Shu, Y.; Jiang, Y.; Zhao, F.; Wei, Y.; Yan, J.; Ren, Y.; Zhou, X.; Liu, Z. Rational design and fabrication of Cu_2O film as photoelectrode for water splitting. *J. Alloys Compd.* **2023**, *956*, 170283. [CrossRef]
27. Yu, X.; Li, X.; Zheng, G.; Wei, Y.; Zhang, A.; Yao, B. Preparation and properties of KCl-modified Cu_2O thin film by electrodeposition. *Appl. Surf. Sci.* **2013**, *270*, 340–345. [CrossRef]
28. Yang, X.; Han, Z.; Song, J.; Hu, P.; Teng, F. Novel application of electrochemical test for the controllable electrodeposition of Cu_2O and metallic Cu film. *J. Alloys Compd.* **2024**, *970*, 172706. [CrossRef]
29. Zhang, Y.; Deng, B.; Zhang, T.; Gao, D.; Xu, A.W. Shape effects of Cu_2O polyhedral microcrystals on photocatalytic activity. *J. Phys. Chem. C* **2010**, *114*, 5073–5079. [CrossRef]
30. Su, Y.; Li, H.; Ma, H.; Robertson, J.; Nathan, A. Controlling surface termination and facet orientation in Cu_2O nanoparticles for high photocatalytic activity: A combined experimental and density functional theory study. *ACS Appl. Mater. Interfaces* **2017**, *9*, 8100–8106. [CrossRef] [PubMed]
31. Yang, Q.; Qin, Y.; Chu, S.; Sun, S.; Liu, D.; Yang, S.; Liang, S. Preparation of nanoporous Cu/Cu_2O composites by anodic oxidation and their electrocatalytic performance towards methanol oxidation. *Mater. Today Commun.* **2021**, *26*, 101992. [CrossRef]
32. Zhang, R.; Li, Y.; Zhang, W.; Sheng, Y.; Wang, M.; Liu, J.; Liu, Y.; Zhao, C.; Zeng, K. Fabrication of Cu_2O/Bi_2S_3 heterojunction photocatalysts with enhanced visible light photocatalytic mechanism and degradation pathways of tetracycline. *J. Mol. Struct.* **2021**, *1229*, 129581. [CrossRef]
33. Uthirakumar, P.; Devendiran, M.; Kim, T.H.; Kalaiarasan, S.; Lee, I.H. Fabrication of flexible sheets of $Cu/CuO/Cu_2O$ heterojunction nanodisks: A dominant performance of multiple photocatalytic sheets under natural sunlight. *Mater. Sci. Eng. B* **2020**, *260*, 114652. [CrossRef]

34. Li, Z.; Xie, G.; Wang, C.; Liu, Z.; Chen, J.; Zhong, S. Binder free Cu_2O/CuO/Cu/Carbon-polymer composite fibers derived from metal/organic hybrid materials through electrodeposition method as high performance anode materials for lithium-ion batteries. *J. Alloys Compd.* **2021**, *864*, 158585. [CrossRef]
35. Yu, L.; Ba, X.; Qiu, M.; Li, Y.; Shuai, L.; Zhang, W.; Ren, Z.; Yu, Y. Visible-light driven CO_2 reduction coupled with water oxidation on Cl-modified Cu_2O nanorods. *Nano Energy* **2019**, *60*, 576–582. [CrossRef]
36. Riveros, G.; León, M.; Ramírez, D. Effect of chloride ions on the structural, optical, morphological, and electrochemical properties of Cu_2O films electrodeposited on fluorine-modified tin oxide substrate from a DMSO solution. *J. Chil. Chem. Soc.* **2016**, *61*, 3219–3224. [CrossRef]
37. Pelegrini, S.; Tumelero, M.A.; Brandt, I.S.; Della Pace, R.D.; Faccio, R.; Pasa, A.A. Electrodeposited Cu_2O modified with Cl: Electrical and optical properties. *J. Appl. Phys.* **2018**, *123*, 161567. [CrossRef]
38. El-Shaer, A.; Darwesh, N.; Habib, M.A.; Abdelfatah, M. Doping of nanostructured Cu_2O films to improve physical and photoelectrochemical properties as a step forward for optoelectronics applications. *Opt. Mater.* **2024**, *148*, 114849. [CrossRef]
39. Pan, L.; Dai, L.; Burton, O.J.; Chen, L.; Andrei, V.; Zhang, Y.; Ren, D.; Cheng, J.; Wu, L.; Frohna, K.; et al. High carrier mobility along the [111] orientation in Cu_2O photoelectrodes. *Nature* **2024**, *628*, 765–770. [CrossRef] [PubMed]
40. Ding, Z.Z.; Tang, X.Q.; Ren, J.C.; Liu, X.Z.; Chen, Y.K.; Xia, Z.Y.; Cao, L.; Chen, X.Q.; Yang, F.J. Tuning the band gaps of ferroelectric Aurivillius compounds by transition metal substitution. *Ceram. Int.* **2020**, *46*, 8314–8319. [CrossRef]
41. Samanta, S.; Yadav, R.; Kumar, A.; Sinha, A.K.; Srivastava, R. Surface modified C, O co-doped polymeric g-C_3N_4 as an efficient photocatalyst for visible light assisted CO_2 reduction and H_2O_2 production. *Appl. Catal. B Environ.* **2019**, *259*, 118054–118072. [CrossRef]
42. Wu, P.; Wang, Y.L.; Zhang, X.C.; Bai, J.Y.; Fu, X.L.; Cao, J.T.; Liu, Y.M. Cu_2O-CuX nanoparticles rich in oxygen vacancies modulated by halogen ions and their application in photocatalytic degradation. *Nanoscale* **2025**, *17*, 15348–15355. [CrossRef] [PubMed]
43. Nosaka, Y.; Nosaka, A. Understanding hydroxyl radical (·OH) generation processes in photocatalysis. *ACS Energy Lett.* **2016**, *1*, 356–359. [CrossRef]
44. González, S.; Jaramillo-Fierro, X. Ab initio study of formation mechanisms and thermochemical properties of reactive oxygen species (ROS) in photocatalytic processes. *Int. J. Mol. Sci.* **2025**, *26*, 8989. [CrossRef] [PubMed]
45. Wang, J.; Liang, Y.; Wang, Z.; Huo, B.; Liu, C.; Chen, X.; Xu, H.; Li, D.; Zhu, Z.; Wang, Y.; et al. High efficiently degradation of organic pollutants via low-speed water flow activation of Cu_2O@MoS_2/PVDF modified pipeline with piezocatalysis performance. *Chem. Eng. J.* **2023**, *458*, 141409. [CrossRef]

Disclaimer/Publisher's Note: The statements, opinions and data contained in all publications are solely those of the individual author(s) and contributor(s) and not of MDPI and/or the editor(s). MDPI and/or the editor(s) disclaim responsibility for any injury to people or property resulting from any ideas, methods, instructions or products referred to in the content.